

Direct Probe of Majorana and Extended Higgs Particles in Radiative Seesaw Models at the ILC

Hiroshi Yokoya

Department of Physics, University of Toyama, Toyama 930-8555, JAPAN

A collider probe of the radiative seesaw models are considered. Two key ingredients of these models, the extended Higgs sector and the source of the Majorana mass, although these details differ model by model, would be studied at the TeV-scale electron-positron and electron-electron colliders. The searches and mass determinations in the inert doublet model, which is the extended Higgs sector of the Ma model, are summarized as an example.

I. INTRODUCTION

The neutrino oscillation data clearly show that neutrinos have tiny masses and large flavor mixing. However, the standard model (SM) cannot explain them, while the masses of the other SM bosons and fermions are accounted for by the Higgs mechanism. Therefore, after the discovery of a Higgs-boson at the LHC, the origin of the neutrino masses and their tininess are imminent questions left to us.

The Majorana masses of the left-handed neutrinos are generated from the dimension-5 effective operators,

$$\mathcal{L} = \frac{c_{ij}}{2\Lambda} \bar{\nu}_L^i \nu_L^j \phi^0 \phi^0, \quad (1)$$

where c_{ij} are dimensionless coefficients, Λ is a cut-off scale above which the internal structure of the vertex may be resolved, and ϕ^0 is the Higgs-boson field. Through the vacuum expectation value of the Higgs boson $\langle \phi^0 \rangle$, the mass matrix for left-handed neutrinos is given as $M_\nu^{ij} = c_{ij} \langle \phi^0 \rangle^2 / \Lambda$. The tiny masses of neutrinos ($M_\nu^{ij} \lesssim 0.1$ eV) mean $c_{ij} / \Lambda \sim \mathcal{O}(10^{-14})$ GeV $^{-1}$ for $\langle \phi^0 \rangle \simeq 256$ GeV. In the tree-level seesaw scenario, it is realized by introducing right-handed neutrinos with Majorana masses of $\mathcal{O}(10^{14})$ GeV and assuming $c_{ij} \sim \mathcal{O}(1)$. On the other hand, radiative seesaw models (RSMs) may be alternative possibilities, in which the small coefficient c_{ij} is realized via the n -loop suppression factor $\sim (1/16\pi^2)^n$ [1–7]. As the results, the cut-off parameter Λ can be much lower than $\mathcal{O}(10^{14})$ GeV, e.g. at the TeV scale. Thus, in such models, direct searches and verification at collider experiments may be possible.

General features of the RSMs are an extension of the Higgs sector and a source of the Majorana mass, although their details are completely model dependent. For example, in the Zee-Babu model [2, 3], $SU(2)_L$ singlet scalars (which have non-zero lepton number) are introduced with their lepton-number-violating interaction to generate the Majorana masses of neutrinos at the two-loop level. The extended Higgs sector in the Ma model [5, 8] is equivalent with the inert doublet model (IDM) [9] where one of the scalar doublet field is Z_2 -odd, and that in the Aoki-Kanemura-Seto (AKS) model [6, 10, 11] is equivalent with the two Higgs doublet model (THDM) with lepton-specific Yukawa interactions [12], with additional $SU(2)_L$ singlet scalars which are odd under the Z_2 -symmetry. As for the Majorana nature, TeV-scale right-handed neutrinos are often introduced in various models, which are Z_2 -odd to avoid the tree-level Dirac mass. The introduced Z_2 -symmetry stabilizes the lightest Z_2 -odd particle in the model. Thus these models naturally contain a candidate of the dark matter.

Collider signatures of the RSMs also differ model by model. To verify the model by experiments, we have to perform direct searches of new particles at colliders, and if discovered, then by measuring their properties and interactions we have to check whether these are enough to describe the neutrino masses. The collider searches of extended Higgs sector have been discussed extensively [13]. On the other hand, the Majorana nature can be probed by direct searches of the TeV-scale Majorana neutrinos [14, 15], or by observing the lepton-number-violated processes, such like the neutrinoless double-beta decay. The searches of right-handed neutrinos in the context of RSMs have been studied in Refs. [16, 17].

II. EXTENDED HIGGS SECTOR IN THE RSMs

Collider signatures of the lepton-specific THDM are characterized by multi- τ production [12, 18, 19], since the extra scalars predominantly decay into τ 's. Such signatures can be observed at the LHC by requiring

appropriate cuts [18]. However, the mass determination would not be straightforward since the reconstruction of the 4τ event kinematics cannot be solved. On the other hand, the 4τ kinematics can be easily solved, and thus the masses and parameters in the model can be determined well at the ILC [19]. The additional SU(2)-singlet scalars in the AKS model may be searched by the energy scan of the production cross-sections of the charged-scalar pair at the ILC [17].

Collider signatures in the IDM are charged leptons plus missing momentum, similar to those of charginos and neutralinos in supersymmetric models. The searches of the inert doublet scalars at lepton and hadron colliders have been studied in Refs. [9, 20–24]. The signatures can be observed at the LHC only if the mass spectrum of the scalars are in favorable cases. On the other hand, at the ILC, the inert doublet scalars can be easily found, unless the masses are too heavy, and precise determinations of the masses and parameters are possible [25]. In the next section, we summarize the detail studies of the searches and mass determination of the additional scalars in the IDM at the ILC based on Ref. [25].

III. INERT DOUBLET MODEL

The IDM is one of the simplest extensions of the Higgs sector in the SM, where an additional SU(2)_L-doublet scalar field is introduced, which is odd under the unbroken Z_2 symmetry [9, 26]. Four kinds of additional scalars appear as physical states, namely neutral CP -even state (H), neutral CP -odd state (A) and charged scalar states (H^\pm), all of which are called inert scalars. Yukawa interactions of the inert scalars to SM fermions are forbidden due to the Z_2 symmetry. Because of the Z_2 -parity conservation, the lightest inert particle (LIP) becomes stable. Therefore, the model provides a scalar dark matter candidate [9, 24, 27–30].

The most general scalar potential can be written as

$$V(\Phi_1, \Phi_2) = \mu_1^2 |\Phi_1|^2 + \mu_2^2 |\Phi_2|^2 + \frac{\lambda_1}{2} |\Phi_1|^4 + \frac{\lambda_2}{2} |\Phi_2|^4 + \lambda_3 |\Phi_1|^2 |\Phi_2|^2 + \lambda_4 \left| \Phi_1^\dagger \Phi_2 \right|^2 + \left\{ \frac{\lambda_5}{2} \left(\Phi_1^\dagger \Phi_2 \right)^2 + \text{H.c.} \right\}, \quad (2)$$

with seven real parameters ($\mu_1^2, \mu_2^2, \lambda_1, \lambda_2, \lambda_3, \lambda_4, \lambda_5$). The potential has to satisfy theoretical constraints, such as the vacuum stability [26] and the perturbativity [9]. By the vacuum stability at the tree level, the quartic terms are constrained as $\lambda_1 > 0$, $\lambda_2 > 0$, $\sqrt{\lambda_1 \lambda_2} + \lambda_3 > 0$, and $\sqrt{\lambda_1 \lambda_2} + \lambda_3 + \lambda_4 - |\lambda_5| > 0$ [26]. We consider the case where $\mu_1^2 < 0$, $\lambda_1 \mu_2^2 > \lambda_3 \mu_1^2$ and $\lambda_1 \mu_2^2 > (\lambda_3 + \lambda_4 + |\lambda_5|) \mu_1^2$ are satisfied [26], so that Φ_2 does not acquire the vacuum expectation value (VEV) and only Φ_1 plays a role of the “Higgs-boson”. By denoting

$$\Phi_1 = \begin{pmatrix} 0 \\ \frac{1}{\sqrt{2}}(v + h) \end{pmatrix}, \quad \Phi_2 = \begin{pmatrix} H^+ \\ \frac{1}{\sqrt{2}}(H + iA) \end{pmatrix}, \quad (3)$$

where v is the VEV, $v = \sqrt{-2\mu_1^2/\lambda_1} (\simeq 246 \text{ GeV})$, the masses of these scalars are expressed as $m_h^2 = \lambda_1 v^2$, $m_{H^\pm}^2 = \mu_2^2 + \frac{1}{2}\lambda_3 v^2$, $m_H^2 = \mu_2^2 + \frac{1}{2}(\lambda_3 + \lambda_4 + \lambda_5)v^2$ and $m_A^2 = \mu_2^2 + \frac{1}{2}(\lambda_3 + \lambda_4 - \lambda_5)v^2$. Thus, the seven parameters in the Higgs potential can be replaced by the VEV v , four masses of the Higgs boson and inert scalars, (m_h, m_{H^\pm}, m_H, m_A), the scalar self-coupling constant λ_2 , and $\lambda_H (\equiv \lambda_3 + \lambda_4 + \lambda_5)$ for example. To force the LIP to be electrically neutral, so that it can be a candidate of the dark matter, $\lambda_4 < |\lambda_5|$ must be satisfied [31]. Depending on the sign of λ_5 , either H or A becomes the LIP.¹ Hereafter, we take H as the LIP.

	Inert scalar masses			ILC cross sections [$\sqrt{s} = 250 \text{ GeV}$ (500 GeV)]	
	m_H [GeV]	m_A [GeV]	m_{H^\pm} [GeV]	$\sigma_{e^+e^- \rightarrow HA}$ [fb]	$\sigma_{e^+e^- \rightarrow H^+H^-}$ [fb]
(I)	65.	73.	120.	152. (47.)	11. (79.)
(II)	65.	120.	120.	74. (41.)	11. (79.)
(III)	65.	73.	160.	152. (47.)	0. (53.)
(IV)	65.	160.	160.	17. (35.)	0. (53.)

TABLE I: Masses of inert scalars and ILC cross sections for our four benchmark points.

¹ In the Ma model, another possibility that the right-handed neutrino becomes the dark matter is not excluded [35]. In such cases,

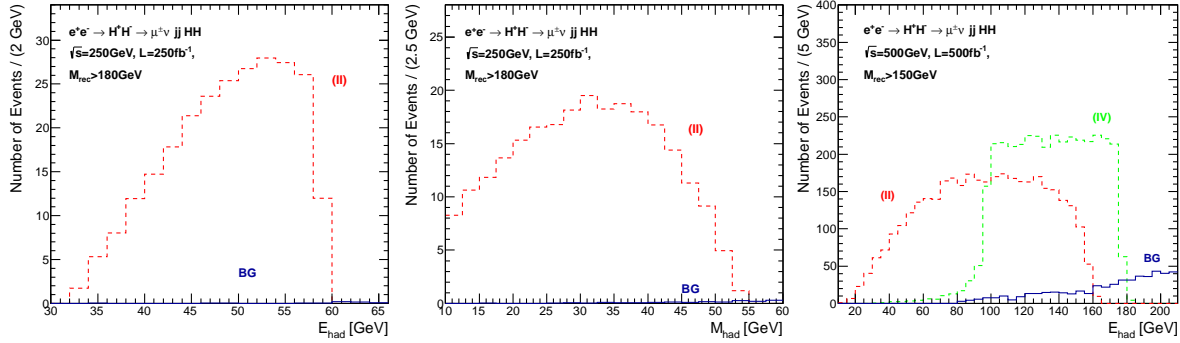


FIG. 1: Distributions of E_{had} , M_{had} in the semi-leptonic decay mode at $\sqrt{s} = 250$ GeV with $\mathcal{L}_{\text{int}} = 250 \text{ fb}^{-1}$ (left and middle) and that of E_{had} at $\sqrt{s} = 500$ GeV with $\mathcal{L}_{\text{int}} = 500 \text{ fb}^{-1}$ (right).

For the collider study, four benchmark points for the masses of inert scalars listed in Table I are considered, which satisfy all the available theoretical and also phenomenological constraints [24]. We study the case where the masses of H and A are close to each other (I, III) for which the LEP and LHC experiments can not probe [20–24]. The other cases are when $m_A - m_H$ is medium (II) or large such that the Z -boson from $A \rightarrow HZ$ becomes on-shell (IV). For the W -bosons in $H^\pm \rightarrow W^\pm H$, we consider the off-shell (I, II) and on-shell (III, IV) cases. For the four benchmark points, the production cross sections of inert scalars at the ILC are large enough to be observed. In Table I, we list the cross sections of HA production and H^+H^- production at $\sqrt{s} = 250$ GeV and 500 GeV.

For the cases (II, IV), H^\pm decays into $W^\pm H$ predominantly, where we admit the W -boson to be off-shell if $m_{H^\pm} - m_H < m_W$. While for the cases (I) and (III), $H^\pm \rightarrow W^\pm A$ decay would be sizable as well, with the branching ratios about 32% and 27%, respectively. The decay of the A -boson is dominated by $A \rightarrow Z^{(*)}H$.

Collider signatures of the inert scalars in the IDM have been studied in the literature [9, 20–24]. In Ref. [21], bounds on the masses of the inert scalars are obtained by using the the LEP II data. Even though the parameter regions where the inert scalars could be discovered at the LHC are pointed out [22–24], detailed analysis on these scalars such as the precise determination of these masses and quantum numbers would be performed at lepton colliders.

$$e^+e^- \rightarrow H^+H^- \text{ process}$$

Here the H^+H^- pair production at the ILC, where H^\pm predominantly decays into HW^\pm , and W^\pm further into $\ell^\pm \nu$ or $q\bar{q}'$ are studied. The semi-leptonic and all-hadronic decay modes are used as successful signatures.

First, we study the semi-leptonic decay mode, where the signature is $\ell^\pm jj$ plus large missing energy. The leading background process would be $\tau^\pm \nu jj$ production followed by the leptonic decay of τ . The $\ell^\pm \nu jj$ background process can be reduced by requiring a large recoil mass. The contribution from production of $\mu^+ \mu^- jj$ and missing particles, where one of the muons goes out of the acceptance region, are negligible. The event simulation for the case (I) [the case (III)] is only differ from that for the case (II) [the case (IV)] by the overall normalization.

In the left and middle panels in Fig. 1, E_{had} and M_{had} distributions in the semi-leptonic decay mode are plotted by using the parameter set (II) at the ILC with $\sqrt{s} = 250$ GeV and $\mathcal{L}_{\text{int}} = 250 \text{ fb}^{-1}$ with a cut of $M_{\text{rec}} > 180$ GeV. For the case with the off-shell W -boson, the endpoints of the all-jets (hadrons) energy

constraints on the parameters, λ_4 and λ_5 , are relaxed.

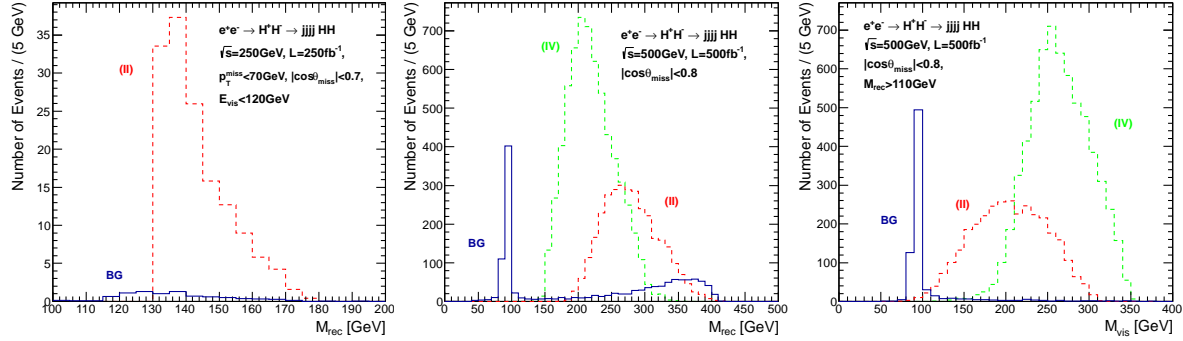


FIG. 2: Distributions of M_{rec} in the all-hadronic decay mode at $\sqrt{s} = 250$ GeV with $\mathcal{L}_{\text{int}} = 250 \text{ fb}^{-1}$ (left), and M_{rec} and M_{vis} distributions in the all-hadronic mode at $\sqrt{s} = 500$ GeV with $\mathcal{L}_{\text{int}} = 500 \text{ fb}^{-1}$ (middle and right).

distribution are given by

$$E_{\text{had}}^{\text{max/min}} = \frac{\sqrt{s}}{4} \left(1 - \frac{m_{H^\pm}^2}{m_{H^\pm}^2} \right) \left[1 \pm \sqrt{1 - \frac{4m_{H^\pm}^2}{s}} \right]. \quad (4)$$

Furthermore, the maximum value of the invariant mass of all hadrons is just the difference between m_{H^\pm} and m_H ,

$$M_{\text{had}}^{\text{max}} = m_{H^\pm} - m_H. \quad (5)$$

In the right panel in Fig. 1, the E_{had} distribution in the semi-leptonic decay modes are plotted by using the parameter sets (II) and (IV) at the ILC with $\sqrt{s} = 500$ GeV and $\mathcal{L}_{\text{int}} = 500 \text{ fb}^{-1}$ with a cut of $M_{\text{rec}} > 150$ GeV. Notice that the parameter set (II) corresponds to the case where H^\pm decays into off-shell W and H , and (IV) corresponds to the case where H^\pm decays into on-shell W and H . When the W -boson is on-shell, the signal distribution is like a rectangle where the edges are given by

$$E_{\text{had}}^{\text{max/min}} = \gamma_{H^\pm} \hat{E}_{\text{had}} \pm \gamma_{H^\pm} \beta_{H^\pm} \hat{p}_{\text{had}}, \quad (6)$$

with $\gamma_{H^\pm} = \sqrt{s}/(2m_{H^\pm})$, $\beta_{H^\pm} = (1 - 4m_{H^\pm}^2/s)^{1/2}$, $\hat{E}_{\text{had}} = (m_{H^\pm}^2 - m_H^2 + m_W^2)/(2m_{H^\pm})$ and $\hat{p}_{\text{had}} = m_{H^\pm}/2 \times \lambda(1, m_H^2/m_{H^\pm}^2, m_W^2/m_{H^\pm}^2)$.

Then, we present the all-hadronic decay mode, which gives the four jets plus large missing energy signatures. Main SM background contributions are the production of four partons with two neutrinos.

In the left panel of Fig. 2, M_{rec} distribution is plotted for the signal process using the parameter set (II) at $\sqrt{s} = 250$ GeV with $\mathcal{L}_{\text{int}} = 250 \text{ fb}^{-1}$. To reduce the SM background, kinematical cuts of $p_T^{\text{miss}} > 70$ GeV, $|\cos \theta_{\text{miss}}| < 0.7$ and $E_{\text{vis}} < 120$ GeV are applied, where θ_{miss} is the polar angle of the missing 3-momenta and E_{vis} is the sum of the energy of all hadrons in one event. As a result, the SM background is sufficiently reduced. The minimum of the M_{rec} distribution is at the twice of m_H ,

$$M_{\text{rec}}^{\text{min}} = 2m_H. \quad (7)$$

In the middle panel of Fig. 2, the same distributions are plotted but for the signal processes using parameter sets (II) and (IV) at $\sqrt{s} = 500$ GeV with $\mathcal{L}_{\text{int}} = 500 \text{ fb}^{-1}$. By the kinematical cut of $|\cos \theta_{\text{miss}}| < 0.8$, the SM background is sufficiently reduced except at $M_{\text{rec}} \simeq m_Z$. The peak of the signal distribution is given by

$$M_{\text{rec}}^{\text{peak}} = \frac{m_H \sqrt{s}}{m_{H^\pm}}. \quad (8)$$

This relation holds even when the W -boson in $H^\pm \rightarrow W^\pm H$ is off-shell [25]. Thus, the ratio of m_H and m_{H^\pm} can be determined.

In the right panel of Fig. 2, the M_{vis} distributions are plotted for the signal processes using parameter sets (II) and (IV) at $\sqrt{s} = 500$ GeV with $\mathcal{L}_{\text{int}} = 500 \text{ fb}^{-1}$. In addition to the kinematical cut applied in the previous

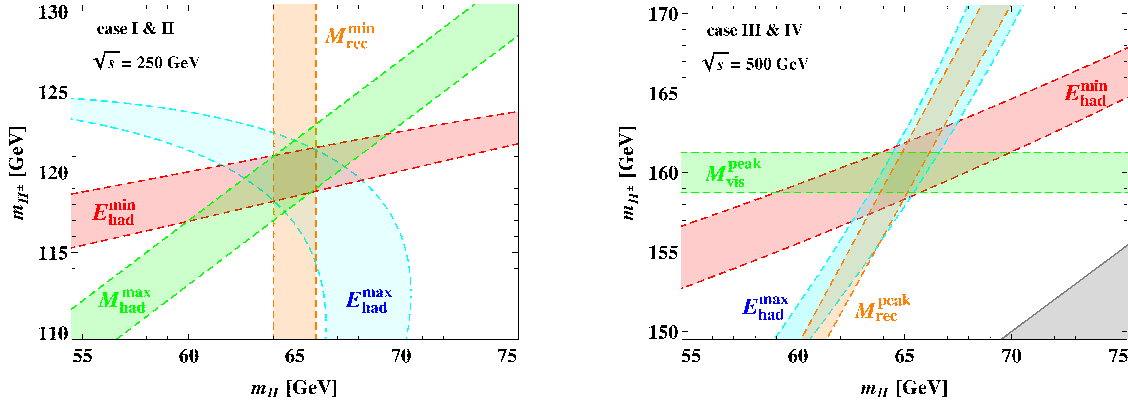


FIG. 3: Determinations of m_{H^\pm} and m_H by the four observables are illustrated in the left [right] panel for the cases (I, II) [(III, IV)] at $\sqrt{s} = 250$ GeV [500 GeV]. Each observable is assumed to be measured in ± 2 GeV accuracy.

panel, the cut of $M_{\text{rec}} > 110$ GeV is applied to reduce the SM background with $Z \rightarrow \nu\bar{\nu}$. After these cuts, the SM background is sufficiently reduced except at $M_{\text{vis}} \simeq m_Z$. The signal distribution has a peak at

$$M_{\text{vis}}^{\text{peak}} = \frac{m_W \sqrt{s}}{m_{H^\pm}}, \quad (9)$$

when the W -boson in $H^\pm \rightarrow W^\pm H$ is on-shell [the case (IV)]. When the W -boson is off-shell, the relation on the peak position no more holds.

The observables for determining m_{H^\pm} and m_H in the process $e^+e^- \rightarrow H^+H^-$ are summarized in Fig. 3. In the left panel, for $m_{H^\pm} - m_H \leq m_W$, the four bands are plotted on the m_{H^\pm} - m_H plane by assuming that the four quantities, $E_{\text{had}}^{\text{max}}$, $E_{\text{had}}^{\text{min}}$ in Eq. (4), $M_{\text{had}}^{\text{max}}$ in Eq. (5) and $M_{\text{rec}}^{\text{min}}$ in Eq. (7), are measured in ± 2 GeV accuracy. For this assumption, the accuracy of the m_{H^\pm} (m_H) determination would be ± 2 GeV (± 1 GeV). On the other hand, if $m_{H^\pm} - m_H \geq m_W$, the four observables, $E_{\text{had}}^{\text{max}}$, $E_{\text{had}}^{\text{min}}$ in Eq. (6), $M_{\text{rec}}^{\text{peak}}$ in Eq. (8) and $M_{\text{vis}}^{\text{peak}}$ in Eq. (9) are utilized for the mass determination. In the right panel of Fig. 3, the four bands are plotted on the m_{H^\pm} - m_H plane by assuming that the four observables are measured in ± 2 GeV accuracy. It turns out that the constraints from measurements of $M_{\text{vis}}^{\text{peak}}$ and $M_{\text{rec}}^{\text{peak}}$ are more stringent than those from the $E_{\text{had}}^{\text{max/min}}$ measurements, if these quantities are measured in an equal accuracy. It is expected that peak positions can be precisely determined more than endpoints of distributions in the presence of the resolution of energy measurements and the remaining background contributions. By combining the four measurements with the uncertainty of ± 2 GeV, m_{H^\pm} and m_H can be determined in ± 1 GeV accuracy.

The discovery of A -boson, the CP -odd inert scalar, is achieved by using the $e^+e^- \rightarrow HA$ process followed by $A \rightarrow HZ$ decay. The study of the collider signature and mass determination in this process can be found in Ref. [25].

IV. MAJORANA NATURE IN THE RSMS

Sometimes, lepton colliders have bigger potential for the direct searches of new particles in the RSMS than hadron colliders. Not only that, to determine the masses and parameters in the model, precise measurements at lepton colliders would be more advanced, since reconstruction of the recoil mass, decay angular distributions and the energy scan of the production cross-sections are possible there. In this report, we have seen that the extended Higgs sector of the RSMS, e.g. IDM or the lepton-specific THDM, can be probed precisely at the ILC.

Furthermore, the Majorana nature in the RSMS can be probed as well at lepton colliders [16, 17]. The t -channel Majorana neutrino exchange diagrams have characteristic contribution to the total cross-section and the angular distributions of the produced particles and their decay products, even though the mass of the t -channel particle is heavier than the scattering energy. An electron-electron collider option at the future ILC experiment would deserve special attention for the direct probe of the RSMS [32–34]. Since the Feynman diagrams of the e^-e^- scattering in the RSMS can be regarded as parts of the diagrams for the neutrino mass generation, it provides the direct test of the Majorana nature in the RSMS.

V. SUMMARY

To summarize, the direct probe of the RSMs at colliders are studied. The key ingredients of the RSMs are the extended Higgs sector and the source of the Majorana mass, while the details are completely model dependent. The collider signatures also differ model by model. It is observed that at lepton colliders not only the extended Higgs sector but also the Majorana nature in the RSMs can be probed.

Acknowledgments

The Author would like to thank Mayumi Aoki and Shinya Kanemura for fruitful collaborations. The work was supported in part by Grant-in-Aid for Scientific Research, No. 24340036.

-
- [1] A. Zee, Phys. Lett. B **93** (1980) 389 [Erratum-ibid. B **95** (1980) 461].
 - [2] A. Zee, Nucl. Phys. B **264** (1986) 99.
 - [3] K. S. Babu, Phys. Lett. B **203** (1988) 132.
 - [4] L. M. Krauss, S. Nasri and M. Trodden, Phys. Rev. D **67** (2003) 085002.
 - [5] E. Ma, Phys. Rev. D **73** (2006) 077301.
 - [6] M. Aoki, S. Kanemura and O. Seto, Phys. Rev. Lett. **102** (2009) 051805.
 - [7] E. Ma and D. Suematsu, Mod. Phys. Lett. A **24** (2009) 583.
 - [8] E. Ma, Mod. Phys. Lett. A **21** (2006) 1777.
 - [9] R. Barbieri, L. J. Hall and V. S. Rychkov, Phys. Rev. D **74** (2006) 015007.
 - [10] M. Aoki, S. Kanemura and O. Seto, Phys. Rev. D **80** (2009) 033007.
 - [11] M. Aoki, S. Kanemura and K. Yagyu, Phys. Rev. D **83** (2011) 075016.
 - [12] M. Aoki, S. Kanemura, K. Tsumura and K. Yagyu, Phys. Rev. D **80** (2009) 015017.
 - [13] J. F. Gunion, H. E. Haber, G. L. Kane and S. Dawson, Front. Phys. **80** (2000) 1.
 - [14] T. Han and B. Zhang, Phys. Rev. Lett. **97** (2006) 171804.
 - [15] J. Kersten and A. Y. Smirnov, Phys. Rev. D **76** (2007) 073005.
 - [16] D. Atwood, S. Bar-Shalom and A. Soni, Phys. Rev. D **76** (2007) 033004.
 - [17] M. Aoki and S. Kanemura, Phys. Lett. B **689** (2010) 28.
 - [18] S. Kanemura, K. Tsumura and H. Yokoya, Phys. Rev. D **85** (2012) 095001.
 - [19] S. Kanemura, K. Tsumura and H. Yokoya, arXiv:1201.6489 [hep-ph].
 - [20] Q. -H. Cao, E. Ma and G. Rajasekaran, Phys. Rev. D **76** (2007) 095011.
 - [21] E. Lundstrom, M. Gustafsson and J. Edsjo, Phys. Rev. D **79** (2009) 035013.
 - [22] E. Dolle, X. Miao, S. Su and B. Thomas, Phys. Rev. D **81** (2010) 035003.
 - [23] X. Miao, S. Su and B. Thomas, Phys. Rev. D **82** (2010) 035009.
 - [24] M. Gustafsson, S. Rydbeck, L. Lopez-Honorez and E. Lundstrom, Phys. Rev. D **86** (2012) 075019.
 - [25] M. Aoki, S. Kanemura and H. Yokoya, arXiv:1303.6191 [hep-ph].
 - [26] N. G. Deshpande and E. Ma, Phys. Rev. D **18** (1978) 2574.
 - [27] L. Lopez Honorez, E. Nezri, J. F. Oliver and M. H. G. Tytgat, JCAP **0702** (2007) 028.
 - [28] E. M. Dolle and S. Su, Phys. Rev. D **80** (2009) 055012.
 - [29] L. Lopez Honorez and C. E. Yaguna, JHEP **1009** (2010) 046.
 - [30] L. Lopez Honorez and C. E. Yaguna, JCAP **1101** (2011) 002.
 - [31] I. F. Ginzburg, K. A. Kanishev, M. Krawczyk and D. Sokolowska, Phys. Rev. D **82** (2010) 123533.
 - [32] T. G. Rizzo, Phys. Lett. B **116** (1982) 23.
 - [33] C. A. Heusch and P. Minkowski, Nucl. Phys. B **416** (1994) 3.
 - [34] G. Belanger, F. Boudjema, D. London and H. Nadeau, Phys. Rev. D **53** (1996) 6292.
 - [35] J. Kubo, E. Ma and D. Suematsu, Phys. Lett. B **642** (2006) 18.